Anisotropy of defect creation in electron-irradiated iron crystals

F. Maury, M. Biget, P. Vajda, A. Lucasson,* and P. Lucasson

Equipe de Recherches du Centre National de la Recherche Scientifique, Laboratoire de Chimie Physique, Bâtiment 350, F-91405 Orsay, France

(Received 8 July 1976)

Single crystals of α-iron were irradiated perpendicularly to the (100), (110), and (111) planes with electrons in the range 0.35–1.7 MeV and their electrical resistivity change rates were measured. A geometrical model of the threshold-energy surface for atomic displacement in a bcc lattice produces a fit to the experimental data leading to the following values for the threshold energies in the principal crystal directions: $T_d^{\langle 100\rangle} = 17 \pm 1$ eV, $T_d^{\langle 111\rangle} = 20 \pm 1.5$ eV, and $T_d^{\langle 110\rangle} \gtrsim 30$ eV. The specific resistivity of a Frenkel pair is deduced to $\rho_F^{Fe} = (30 \pm 5)$ $\mu\Omega$cm/at.%. From the obtained T_d's we derived an interatomic potential of the Born-Mayer type, valid in the range $1.2 \leq r \leq 2.5$ Å. We propose as a good choice: $V(r) = 8900e^{-4.5r}$ eV. The recovery due to isochronal annealing during stage I, after irradiation at different electron energies, was measured and related to specific recovery mechanisms. Thus, the first important substage, I_B (~ 66 K), is due to the recovery of close Frenkel pairs created in the ⟨100⟩ direction, while a comparison of calculated cross sections suggests that I_C (~ 87 K) possibly stems from ⟨111⟩ close pairs. Substage I_D (90–110 K) is complex; its first part, below 100 K, originates mostly from defects produced in the ⟨100⟩ direction and the second part, above 100 K, together with I_E, principally originates from defects produced in the ⟨111⟩ direction.

I. INTRODUCTION

Encouraging progress has been achieved in the study of radiation damage in single crystals since the pioneering work of the Brookhaven computer group on copper[1] and iron.[2] A whole series of fcc, bcc, and hcp metals has been analyzed in more or less sophisticated experiments and information concerning their threshold energy surface for atomic displacement has been furnished. (The latest state of the art has been presented in a recent review article by one of the authors.[3]) The first experimental work on damage anisotropy in bcc crystals was done by Lomer and Pepper[4] on α-iron, who irradiated specimens with electrons perpendicularly to the (100) and the (111) planes, respectively, in an attempt to verify the computer predictions of Erginsoy *et al.*,[2] who had found a minimum displacement threshold in the ⟨100⟩ direction. Comparing the shapes of their defect production curves as a function of electron energy and using a geometrical model for displacements in a bcc lattice, which was a result of an adaptation of the computer findings,[2] Lomer and Pepper[4] had been able to derive a simplified threshold energy surface for iron. The cross sections for displacement computed with this surface gave a best fit to experiment with $T_d^{\langle 100\rangle} = 20$ eV and $T_d^{\langle 110\rangle} = T_d^{\langle 111\rangle} = 30$ eV. A major drawback of this work was the fact that, due to experimental difficulties, only normalized data were available for the (100) and the (111) crystals while results on (110) crystals were entirely lacking. A detailed investigation of another bcc metal, tantalum, has been undertaken by Jung and Schilling,[5] who had determined its T_d surface by irradiating specimens along many crystallographic orientations; they found minimum T_d's in directions slightly off the principal axes and, in particular, the lowest T_d near ⟨111⟩—rather in contradiction with the computer findings[2] and the experimental results[4] on α-iron. Further thorough work has been performed by the present authors on molybdenum[6,7] where, once more, the lowest T_d has been observed in the ⟨100⟩ direction, while $T_d^{\langle 111\rangle}$ was about 30% higher than $T_d^{\langle 100\rangle}$ and only half of $T_d^{\langle 110\rangle}$. A very important result of this work was the observation of anisotropy of the stage-I recovery spectrum of molybdenum[6] whose manifestations had been related to the anisotropy of the T_d surface.[7] (Early work on recovery anisotropy had been done by Cusson *et al.*[8] with iron whiskers, but the observations were not very conclusive because of the great thickness of the specimens.) Very recently, Dausinger and Schultz[9] have reported data concerning the recovery anisotropy in stage I of electron irradiated tungsten crystals, which are qualitatively similar to those obtained with monocrystalline molybdenum.[6]

The purpose of this work was to check and to complete the experimental results of Lomer and Pepper[4] in view of establishing a threshold-energy surface for α iron based on more detailed data. A simultaneously undertaken investigation of the stage-I recovery spectrum of the three irradiated orientations (100), (110), and (111) should—after determination of the principal displacement mechanisms—permit the attribution of various substages to the annealing of specific Frenkel pairs. Finally, we shall try to determine the interatomic

potential in iron (in a limited range) by calculating—as it had been done with molybdenum[7]—the energies needed to propel an atom through different "lenses" of the bcc lattice and matching them to the previously derived threshold energies.

II. EXPERIMENTAL TECHNIQUES

Roughly 1-mm-wide strips were cut out on a diamond-blade saw parallel to the crystallographic planes (100), (111), and (110) from single-crystal iron platelets obtained by courtesy from Dr. B. Thomas, Institut de Recherches Sidérurgiques (St. Germain en Laye). After a mechanical polish to ~150 μm, they were thinned chemically in a solution of 95 vol.% H_2O_2 + 5 vol.% HF to a final thickness of 20–40 μm, the other dimensions being ~14×0.5 mm. Afterwards, the specimens were annealed for 4 h at 800 °C in a vacuum of 10^{-9} Torr. All the pertinent information concerning the final specimen characteristics is given in Table I.

The crystals were mounted on an insulated holder in a liquid-helium cryostat[10] modified such as to permit irradiations in a vacuum. (The traditional sample chamber where helium was circulated to ensure low irradiation temperatures and which, therefore, was separated from the beam tube by a metallic window would cause too much beam straggling for the electrons at the low expected threshold for iron, E_d = 300–350 keV.) Fortunately, the annealing of damage in iron begins at rather high temperatures[11] and only a few percent of the induced damage recovered at the irradiation temperature. The damage was monitored by measuring the electrical resistivity changes at a temperature stabilized in the region 5–6 K, with a sensitivity of the order of 10^{-11} Ω cm. The irradiation was performed at a temperature around 36 K, measured by the resistivity of the irradiated specimens themselves. The electrons were extracted from a Cockroft-Walton vertical accelerator, their energy was varied between 0.35 and 1.7 MeV; the beam homogeneity was assured by a beam sweep system. The isochronal recovery measurements up to 125 K were performed *in situ*, in 10-min pulses. (The limited number of points was related with the long time necessary to obtain a stable measuring temperature in the evacuated sample chamber.)

TABLE I. Specimen characteristics.

Sample	Thickness in μm	$\rho_{295}/\rho_{4.2\ K}$	Mean[a] thickness
(100)	18–27	55	22
(110)	20–40	45	28
(111)	20–40	37	28

[a] Deduced from the measured resistance.

III. RESULTS AND DISCUSSION

A. Defect production

1. Experimental results

Two series of irradiations were performed independently with two sets of samples, each set including two specimens parallel to the (100) plane, two specimens parallel to the (111) plane, and one specimen parallel to (110). The whole of the experimental results concerning the defect production is displayed in Fig. 1. For each orientation, the data relative to different specimens have been normalized together by a factor which depends on the homogeneity of the samples (width and thickness). In the case of fairly homogeneous samples, the production rates were reproducible from one sample to another within 15%. In the case of less homogeneous samples, the discrepancy could be much higher due to a wrong estimate of the shape factor used for transforming the measured resistance changes into resistivity changes, but the shapes of the curves remained the same as shown experimentally. (This is because the weakest regions of the samples, consecutive to electropolishing, occurred at the ends of the samples, generally outside the irradiated area.)

The inserts in Fig. 1 present an enlarged view of the low-energy part of the curves (ten irradiations were performed at 0.4 MeV and 15 and 0.45 MeV). The production curves for the three irradiated orientations are shown together in Fig. 1d. The three curves converge towards the same apparent threshold energy around 330 keV, which corresponds to a maximum transmitted energy T_m = 17 eV. Yet, the higher production rate below 0.4 MeV for the (100) samples clearly indicates that the crystallographic direction of minimum threshold energy is ⟨100⟩, as predicted by Erginsoy's calculations[2] and confirmed by Lomer's experiments.[4]

2. Analysis of the results

The analysis of the results was done on the basis of the geometrical model already used for molybdenum and described in detail in Ref. 7. Yet, in the case of iron, two points are to be underlined:

(i) the threshold for the incident electrons is much lower than in the case of molybdenum, thus resulting in an important dispersion of the beam through the sample and leading to the same apparent threshold energy for all orientations as shown in Fig. 1(d);

(ii) the samples were irradiated in vacuum to

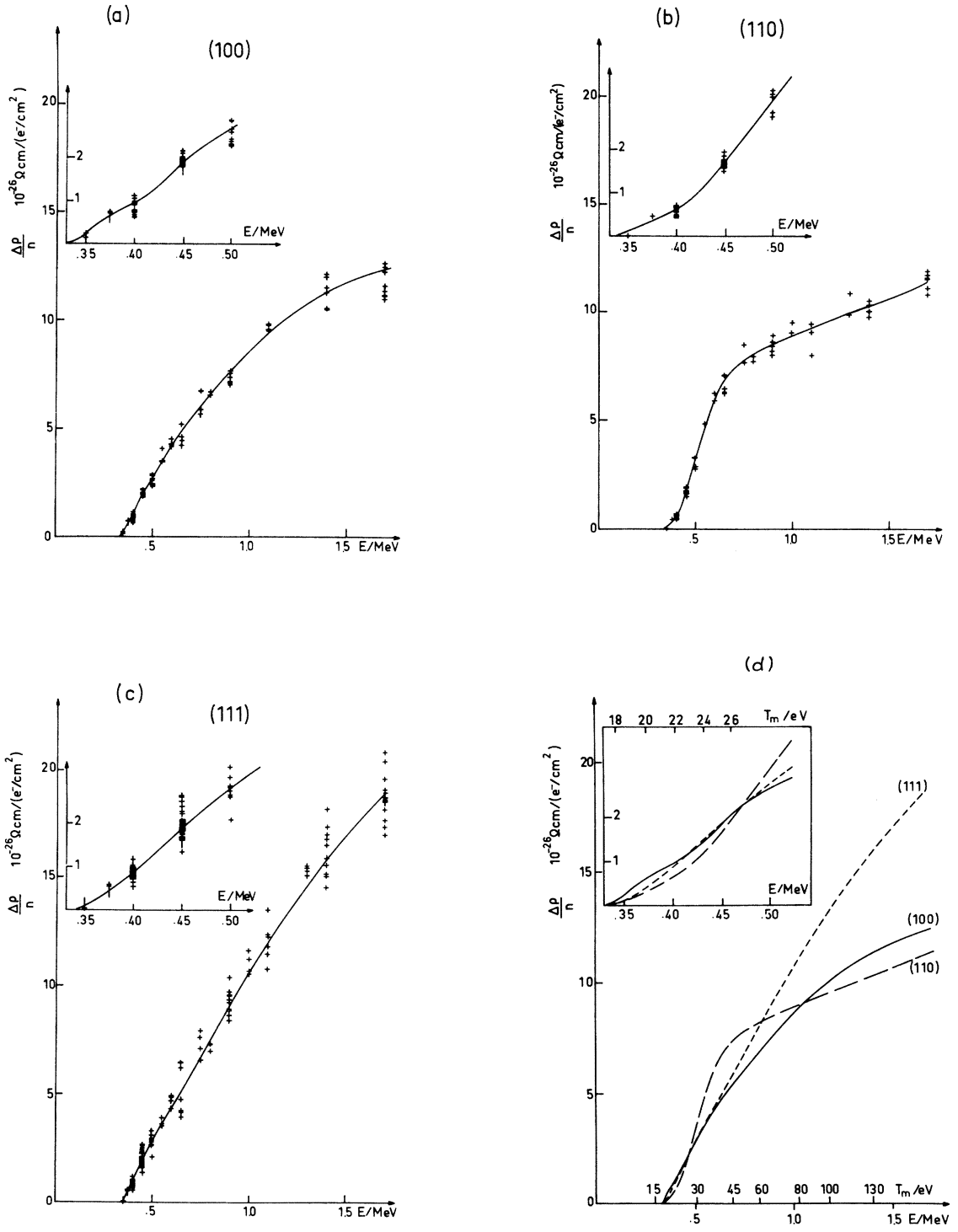

FIG. 1. Electrical resistivity change rates as a function of incident electron energy for three orientations of iron crystals: (100)—curve a, (110)—curve b, (111)—curve c. The inserts present enlarged views of the low-energy part of the curves. The solid lines are eye fits through the experimental points. These fits are drawn together in Fig. 1 (d). On this figure, we have indicated on the abscissa the maximum transmitted energy T_m corresponding to the electron energy E.

minimize beam dispersion; this causes the dispersion to become highly nonuniform throughout the sample, starting from zero to reach a mean angular deviation of ~50° (calculated according to the formulation by Mott and Massey[12]) at a thickness $x = 30\ \mu$ for an energy $E = 0.35$ MeV.

For these two reasons, the calculation of the displacement cross sections has been modified in order to take into account the angular dispersion and the energy loss of the beam as a function of its penetration into the sample. The bases of the applied corrections are explained in Ref. 13; the method was the same as used for the polycrystal experiments and is described in detail in Ref. (14). The damage rate as a function of E is $\Delta\rho(E)/n = \rho_F \sigma(E)$. The displacement cross section $\sigma(E)$ is calculated for various depths in the sample, according to the formula

$$\sigma(E) = \sum \frac{1}{x_0} \int_0^{x_0} \alpha(x)(1 + 2kx)\sigma(\bar{E}(x))\, dx\ ,$$

where x_0 is the average thickness of the sample. The summation is extended over the various "windows" of the threshold energy surface, each one corresponding to displacements into a given crystallographic direction with a constant threshold energy. $\alpha(x)$ is the fraction of the incident electrons which have, at a depth x, an energy greater than the threshold energy. $\bar{E}(x)$ is the mean energy of these electrons; $\sigma(\bar{E}(x))$ is the McKinley-Feshbach differential cross section, integrated over all the directions for an energy $\bar{E}(x)$ of the impinging electrons. Figure 2(a) shows, for the ⟨100⟩ displacements only, and assuming a threshold energy $T_d^{\langle 100\rangle} = 17$ eV, the calculated cross sections as a function of depth in different cases (two samples and three energies). Figure 2(b) shows, for the same samples, the cross sections as a function of energy, calculated with (solid line) and without (dashed line) the above corrections, in the latter case for a mean depth equal to half the sample thickness.

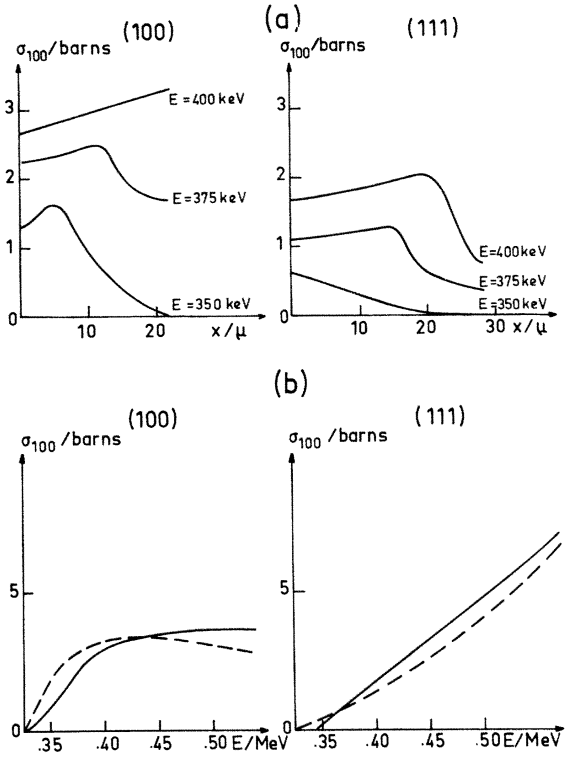

FIG. 2. (a) Calculated cross sections for two orientations and for different energies near threshold, as a function of the pentration depth in the sample. (b) Displacement cross sections for the (100) and the (111) orientations as a function of the incident electron energy, calculated with (solid lines) and without (dashed lines) corrections for energy loss and beam straggling.

3. *Determination of the threshold energies*

We used the same threshold-energy surface as in the case of molybdenum,[7] except for some slight modifications of the window dimensions (low-threshold regions around the main crystallographic directions): the opening of the ⟨100⟩, ⟨111⟩, and ⟨110⟩ windows were set equal to 18°, 19°, and 10×20°, respectively, instead of 22°, 26°, and 5×20°, in order to improve the fit to the experimental results. As pointed out by Jung,[5] changing the size of the windows does not change the set of values for the threshold energies which leads to the best fit, although it may change much the quality of the fit. Our best fit is illustrated in Fig. 3(a). It was obtained with

$$T_d^{\langle 100\rangle} = 17\ \text{eV},\quad T_d^{\langle 111\rangle} = 20\ \text{eV},\quad T_d^{\langle 110\rangle} = 35\ \text{eV}.$$

The ratios of these values are roughly the same as those deduced for molybdenum.[7] The ⟨111⟩ threshold energy is surprisingly low compared to Erginsoy's calculations.[2] As in the case of molybdenum, the matching gives quite satisfactory agreement except for the (100) sample in the medium-energy range, where the experimental production curves exhibit in both cases (Mo and Fe) a bump which is never reproduced by the calculations. This may come from the oversimplification we are making in the definition of the threshold energy surface; the bump would then indicate a more complicated shape of the T_d surface around the ⟨100⟩ direction. Since we are taking into account the energy losses and the beam scattering, the determination of the lowest threshold energy can be done with a precision of ±1 eV,

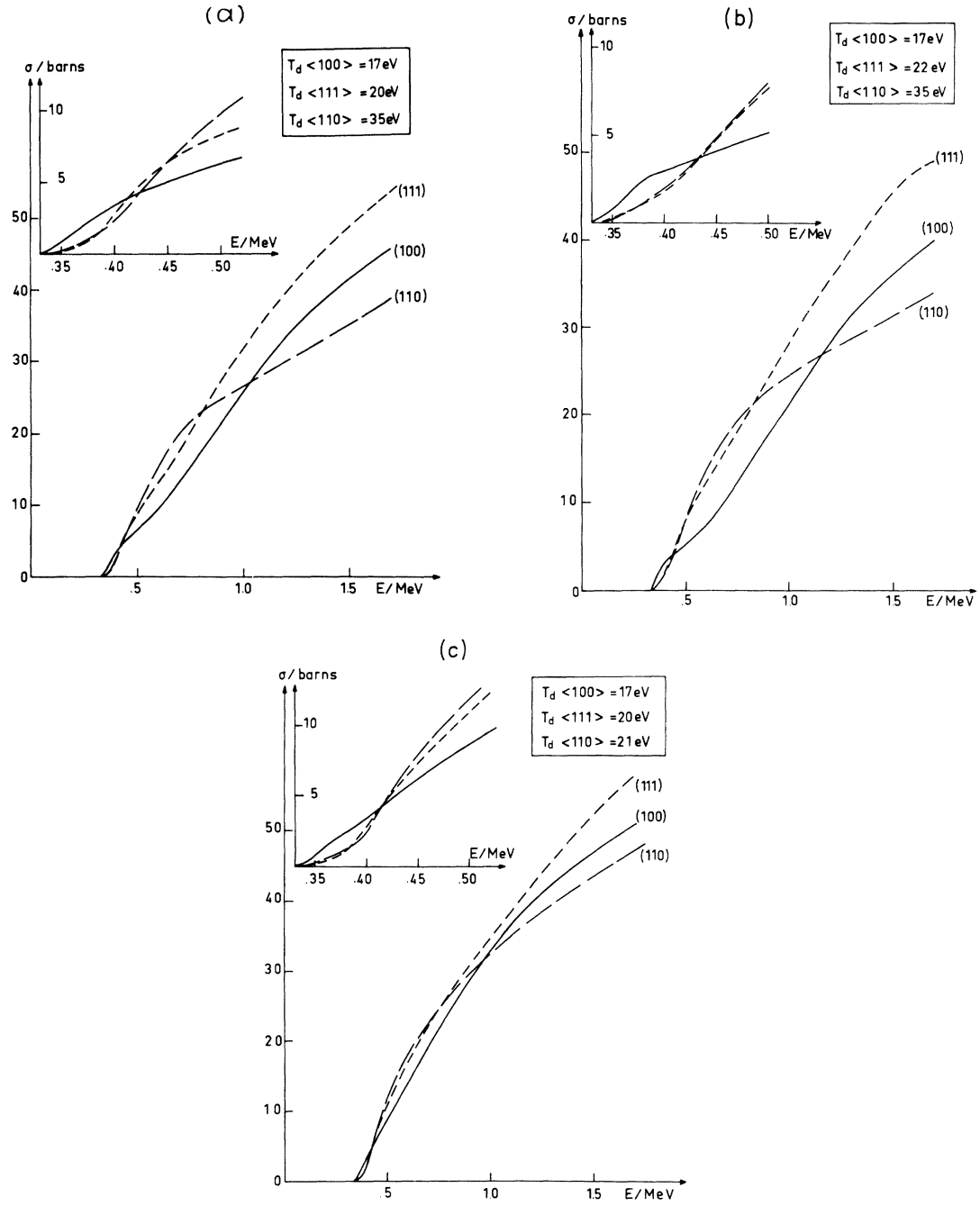

FIG. 3. Displacement cross sections calculated using various sets of threshold energies as parameters.

which is comparable to the one achieved in our polycrystal experiments.[14]

The influence of a variation in $T_d^{\langle 111\rangle}$ is illustrated in Fig. 3(b). The determination of a second threshold energy which is not very different from the lowest T_d necessitates a detailed knowledge of the experimental production rates in the low-energy range. The precision on $T_d^{\langle 111\rangle}$ is estimated to better than ±1.5 eV.

The threshold in the ⟨110⟩ direction is determined with a much smaller accuracy, due to its relatively high value as well as to the small opening of the ⟨110⟩ lenses. We tried to decrease $T_d^{\langle 110\rangle}$ in order to increase the production rates for the (100) sample in the medium energy range. The result is shown in Fig. 3(c): the fit is worsened, especi-

ally as concerns the shape of the (110) curve. The only statement which can reasonably be made on $T_d^{\langle 110\rangle}$ is then $T_d^{\langle 110\rangle} \gtrsim 30$–$35$ eV.

4. *Frenkel-pair resistivity*

The Frenkel-pair resistivity is deduced to be $\rho_F = 30 \pm 5$ $\mu\Omega$cm/at.%. For instance, the fit of Fig. 3(a) was obtained for $\rho_F = 30\,\mu\Omega$cm/at.%, the fit of Fig. 3(b) for $\rho_F = 26.5\,\mu\Omega$cm/at.% and the one of Fig. 3(c) for $\rho_F = 25\,\mu\Omega$cm/at.%. Smaller values of the threshold energies lead to smaller values of ρ_F. ρ_F is also dependent on the shape of the threshold energy surface: increasing the size of the windows decreases ρ_F.

The value we obtain is not far from $\rho_F = 3\rho_0 = 29$ $\mu\Omega$cm, where ρ_0 is the resistivity of iron at 0 °C. It is 50% larger than the one determined by Cusson, Lucasson, and Walker.[8] It is larger, too, than the values given by the empirical rules[15]: $\rho_F \approx \rho(\theta) = 20\mu\Omega$cm, where θ is the Debye temperature, and $\rho_F \approx 0.15\rho(T_m) = 19.5$ $\mu\Omega$cm, where T_m is the melting point. To this higher value of ρ_F will correspond a higher value of the spontaneous recombination volume, determined experimentally from the saturation value of the irradiation induced resistivity. Thus, employing $\rho_F = 12.5$ $\mu\Omega$ cm/at.%, Horak and Blewitt[16] deduced a recombination volume under fast-neutron irradiation of 54 atomic volumes (according to the model of Lück and Sizmann[17]). This value becomes 130 at.vol. if $\rho_F = 30$ $\mu\Omega$cm/at.%; this is still lower than that for most other metals.

5. *Deduction of an interatomic potential*

We are looking for an empirical potential given in a Born-Mayer form: $V(r) = Ae^{-br}$, to be valid in the range $\frac{1}{2}a_0 < r < a_0$, where a_0 is the nearest-neighbor distance. The calculation of the threshold energies in the various crystallographic directions, as described in Ref. (7), enables us to determine the two parameters A and b. On Fig. 4, A is plotted as a function of b such as to lead to a threshold energy in the ⟨100⟩ direction $T_d^{\langle 100\rangle} = 17$ eV, either after two lens passages (dashed line) or after three lens passages (solid line). The corresponding distance between interstitial and vacancy is $\lesssim 4a$ in the former case and $\lesssim 6a$ in the latter, where $2a = 2.86$ Å is the cube-cell side. For each pair (A, b), the Fig. 4 shows the calculated threshold energy in the ⟨110⟩ direction (assuming one or two lens passages) and the number $[n]$ of replacements needed in the ⟨111⟩ direction in order to get $T_d^{\langle 111\rangle} = 20$ eV. In the former case, dashed curve, this number has a maximum value of 6 for $b = 2.9$ Å^{-1}. The corresponding recombination volume is around 60 at. vol., a low value in view of what has been discussed above, even if one considers that the recombination volume might be smaller under electron irradiation than under neutron irradiation. Neither the consideration of the recombination volume nor the value of $T_d^{\langle 110\rangle}$ allow us to choose precisely between all the potentials of the second curve (solid line). The large values for b—around 4.5 Å^{-1}—will give a potential leading to a recombination volume of $\gtrsim 110$ at. vol. ($[n] = 5$); the smaller values for b will give rise to longer-range interactions in the ⟨111⟩ direction ($[n] = 9$), thus leading to a slightly larger recombination volume – $\gtrsim 130$ at.vol. The two limiting cases: $b = 4.5$ Å^{-1}, $A = 8900$ eV (curve a), and $b = 3.0$ Å^{-1}, $A = 570$ eV (curve b) are presented in Fig. 5 together with different other iron potentials used in the literature.[2,18–22] Our steeper potential (curve a) comes very near to the one used by Erginsoy,[2] which had been obtained by fitting the elastic constants of iron, and to that proposed by Andersen and Sigmund[18] following a scaling analysis of displacement-threshold experiments on several cubic metals. Furthermore, in the interesting energy range of 1–10 eV, it is quite close to the potentials of Johnson[20] and of Bullough and Perrin.[21] For this reason, and inasmuch as the measured recombination volume remains unusually small in the case of iron com-

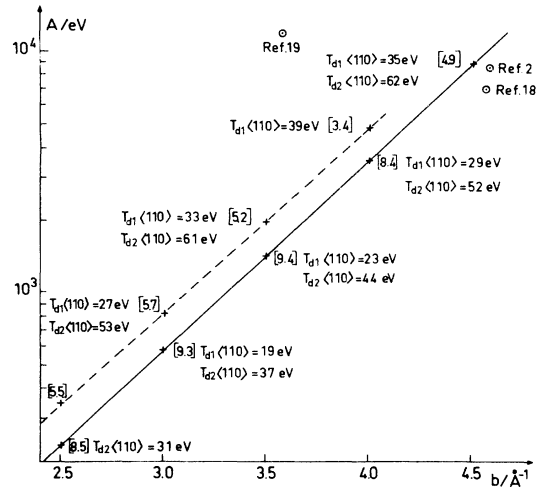

FIG. 4. Relations between the Born-Mayer potential constants A and b so as to yield $T_d^{\langle 100\rangle} = 17$ eV, either after two (dashed line) or after three (solid line) lens passages in the ⟨100⟩ direction. The framed numbers indicate for each pair (A, b) the corresponding number of lens passages in the ⟨111⟩ direction to give $T_d^{\langle 111\rangle} = 20$ eV. The threshold in the ⟨110⟩ direction is given for one (T_{d1}) or two (T_{d2}) passages.

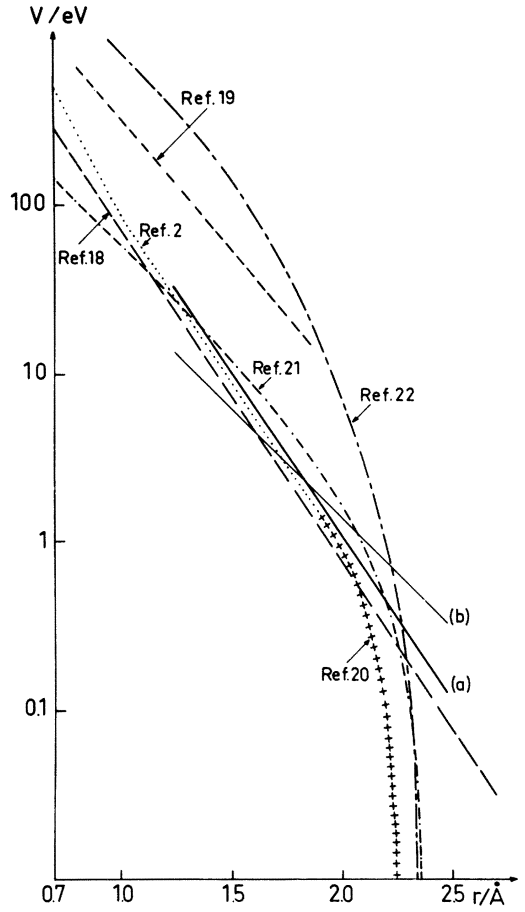

FIG. 5. Various interatomic potentials for iron. Potentials (a) and (b) are taken out of Fig. 4. They correspond to $A = 8900$ eV, $b = 4.5$ Å^{-1} [curve (a)] and to $A = 570$ eV, $b = 3.0$ Å^{-1} [curve (b)].

pared to other metals, we prefer to adopt the potential

$$V = 8900e^{-4.5r} \text{ eV}.$$

B. Stage-I recovery

A first isochronal anneal (with $\Delta t = 10$min and $\Delta T = 4$ K) was performed after an irradiation at 1.7 MeV, the irradiation temperature being < 30 K. The results are not shown here, since at this high energy ($T_m = 178$ eV $= 10.5 T_d^{\min}$) no anisotropy was observed (like in Cusson's experiment[8]). In this run, 2–3% of the damage recovered between the irradiation temperature and 36 K and about the same percentage between 36 and 56 K. The following irradiation, with $E = 0.4$ MeV, was performed at $T_{irr} < 15$ K: no observable recovery was noted below 60 K. The irradiation temperature was then fixed to 36 K, since it is not possible to ascribe any interpretation to recovery peaks which amount to a few percent only of the total damage.

Two isochronal anneals were performed after irradiations at 0.65 and 0.45 MeV (with $\Delta t = 10$ min and $\Delta T = 5$ K except for the first two points). The results are shown in Figs. 6(a) and 6(b). A few points were measured after an irradiation at 0.4 MeV and are shown in Fig. 6(c). These three curves have been normalized to the total recovery measured at 125 K, the presumed temperature of the end of stage I.

1. Substage I_B, between 55 and 75 K

The positions of the main recovery peaks are known from the polycrystal experiments (see,

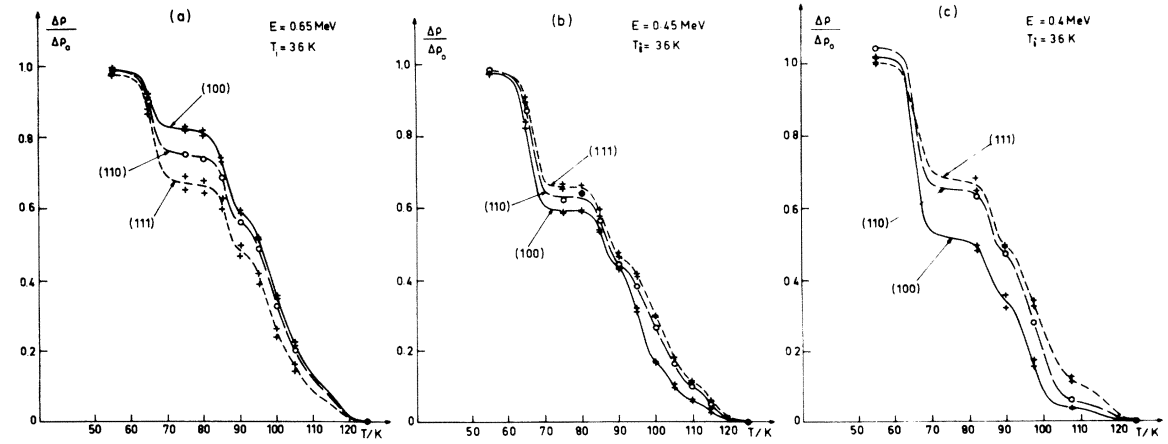

FIG. 6. Isochronal recovery spectra for various samples of different orientations after irradiation with 0.65 MeV (a), 0.45 MeV (b), and 0.4 MeV (c) electrons at a temperature of 36 K; $\Delta t = 10$ min. The curves are normalized to 125 K.

e.g., Minier,[23] Neely and Keefer,[24] Leveque *et al.*[25]). The first important substage, centered around 66 K, has been attributed to the recovery of close Frenkel pairs.[23] Our results clearly demonstrate that the close pairs responsible for the substage I_B are produced in the ⟨100⟩ direction. This is derived from the following two observations:

(i) at low energies [see e.g., Fig. 6(c) where $E = 0.4$ MeV corresponding to a maximum transmitted energy $T_m = 22$ eV $= 1.3\ T_d^{\min}$] the relative importance of substage I_B is maximum for the (100) samples:

(ii) as one increases the energy, the relative amplitude of substage I_B decreases for the (100) samples while it increases for the (111) samples, till a complete inversion is observed at 0.65 MeV where $T_m = 42$ eV $= 2.5\ T_d^{\min}$. (This is due to the Rutherford scattering cross section, which favors the collisions where the target particle is ejected at a large angle from the incident particle.)

The activation energy for this substage had been found to be 0.19 eV[21] in the chemical-kinetics model, the reaction order being one. This value fits our results within the experimental error as can be seen in Fig. 7, while the value of 0.10 eV deduced recently by Wells and Russel[26] gives a slightly too broad substage. (The points on Fig. 7 are experimental points, whereas the curves are calculated assuming different values for the activation energy. The shape of substage I_B is found to be independent of the sample orientation, although its relative amplitude depends very much on it; only the (100) data are shown on the figure.)

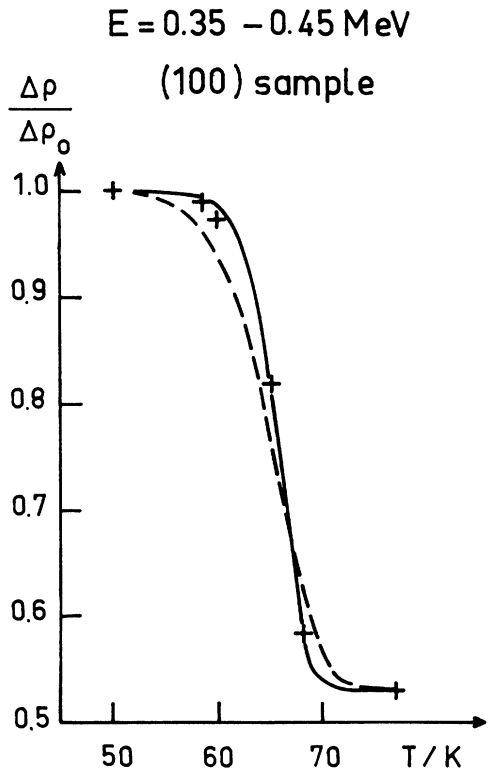

FIG. 7. I_B substage. The crosses are experimental points measured for a (100) sample after an irradiation at 0.35–0.45 MeV. The curves are calculated assuming a first-order reaction and an activation energy of 0.10 eV (dashed line) and 0.19 eV (solid line).

2. *Substage I_C, centered around 87* K

The substage I_C has been shown to be independent of dose, vacancy concentration[24] or impurity concentration[25]; it is, thus, attributed to the recovery of close Frenkel pairs. This substage is not clearly separated from the substage I_D and, for this reason, is difficult to analyze. Moreover, and surprisingly, it does not depend much on the crystal orientation either, nor on the irradiation energy (cf. Fig. 6). Our recovery curves may not go into enough detail to show this dependence clearly—if it does exist. Yet, one can assume that the same pairs, recovering in substage I_C, can be produced by two different mechanisms, the originating knock-on being directed either in the ⟨100⟩ or in the ⟨111⟩ direction (and resulting in both cases in a pair created in the ⟨110⟩ direction, for example); or one can assume that two different kinds of pairs, created in two different directions, annihilate in the same temperature range—in this case, their dependence on orientation and on energy would cancel each other.

3. *Substage I_D, between 90 and 110* K

It has already been noted, and one can see it from the recovery curves of Refs. (24) and (25), that substage I_D is complex. This is manifest, too, on Fig. 6(b), for example, where the shape of I_D is seen to vary with the sample orientation. Besides, as our specimens are not of high purity ($\rho_{4.2\ K} = 200$–$300\ n\Omega$cm), substage I_E is shifted towards the low temperatures and appears only as a shoulder on the I_D peak between 110 and 125 K. Like substages I_B and I_C, substage I_D does not depend on dose, vacancy concentration[24] or impurity concentration.[25] Its activation energy has been found[27] to be equal to 0.32 eV in the whole temperature range 96–128 K (including the I_E peak).

One can, therefore, attribute the I_D peak to the correlated recovery of the freely migrating interstitial, the number of jumps depending on the distance between the interstitial and its vacancy. If one compares the recovery curves at 0.4 MeV

[Fig. 6(c)] for the (100) and the (111) samples, one can see that the decrease of substage I_B when going from the (100) to the (111) orientation is compensated by a relative increase of the two substages I_D and I_E. In fact, I_D is not increased as a whole: only the second part of it (above 100 K) is increased whilst the first part even shows a slight decrease. This can be interpreted in the following way: A low-energy irradiation (here, $T_m = 1.3T_d^{\min}$) produces in a (111) sample—as compared to the (100) sample—less pairs in the ⟨100⟩ direction and more pairs in the ⟨111⟩ direction. Thus, the first part of substage I_D must arise mostly from ⟨100⟩ pairs, while the second part of I_D (above 100 K) as well as I_E stem mainly from ⟨111⟩ pairs. This implies that the mean separation distance between the interstitial atom and its own vacancy is larger for the ⟨111⟩ pairs than for the ⟨100⟩ ones and that this difference can account for the observed width of substage I_D.

If one considers the different curves of Fig. 6, one can verify that it is impossible to fit the whole substage I_D with a single peak of first order and activation energy of 0.32 eV, but a fit can be obtained with two peaks (of first order and same activation energy) centered at 96 and at 104 K (as can be seen in Fig. 8) or with any combination of more than two peaks centered within a temperature interval of ~ 10 K. This temperature gap between the outermost possible component peaks corresponds to a ratio of the respective mean numbers of jumps of ~ 40, and thus to a ratio of

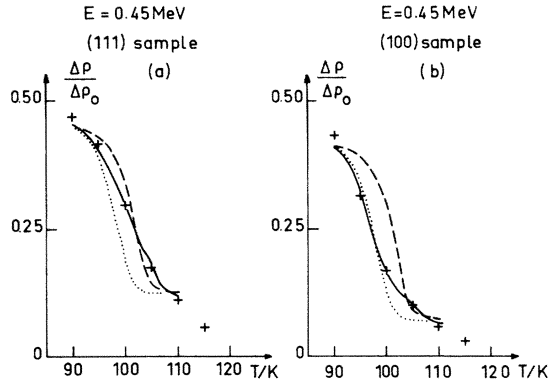

FIG. 8. I_D substage. The crosses are experimental points measured for a (111) sample [curve (a)] and a (100) sample [curve (b)] after an irradiation at 0.45 MeV. The curves are calculated assuming a constant activation energy in the whole temperature range $E_a = 0.32$ eV, and: a single peak of first order centered at 98 K (dotted lines); a single peak of first order centered at 102 K (dashed lines); two peaks of first order centered at 96 and at 104 K the amplitudes of which are respectively 0.13 and 0.21 in case (a) and 0.24 and 0.12 in case (b) (solid lines).

the mean separation distances (for the closest ⟨100⟩ pairs and the most distant ⟨111⟩ pairs that recover in substage I_D) of ~3.5. At 0.45 MeV, the maximum transmitted energy is $T_m = 25.4$ eV, and the maximum number of passages in the ⟨111⟩ direction corresponding to it (calculated with the potential of Sec. A.5) is 11, which means a separation distance of $19a$. With the same potential, the minimum separation distance of ⟨100⟩ pairs is $6a$, but these pairs are likely to annihilate before stage I_D. We are thus left with a minimum distance of $8a$ for the ⟨100⟩ pairs of substage I_D. These two numbers are in a ratio of 2.4, which is somewhat smaller than the just found value of 3.5.

4. *Comparison with calculated cross sections*

The fact that the various substages of stage I are not separated well enough to determine their relative amplitudes (except for I_B) makes it difficult to compare the measured amplitudes to calculated percentages of displacements in the main crystallographic directions. Yet, we have given in Table II the percentages of ⟨111⟩ displacements calculated for two cases (i) $T_d^{\langle 100\rangle} = 17$ eV and $T_d^{\langle 111\rangle} = 20$ eV, (ii) $T_d^{\langle 100\rangle} = 16.5$ eV and $T_d^{\langle 111\rangle} = 19$ eV, together with the measured amplitude of (i) the recovery between 100 and 125 K, (ii) the recovery between 100 and 125 K plus the recovery between 75 and 90 K (I_C). One notices that at low energies the calculated percentages are very dependent on the chosen threshold energies, since a slight modification of the latter gives rise to a non-negligible change in the former. At high energies, the calculation is not so directly comparable with the experimental results, since it cannot account for the multiple displacements. Morever, at 0.65 MeV, we did not consider the pairs created in the ⟨110⟩ direction [(3–9)% of the total production], since we are not able to associate them with the recovery in any particular temperature range.

This comparison between experimental data and calculated results (illustrated by Table II) does not allow us to make any definite attribution of substage I_C. Yet the agreement obtained in the case (ii) seems more satisfactory; this would imply that the pairs which recover during I_C are close pairs produced in the ⟨111⟩ direction.

Let us now come back to the pairs produced in the ⟨100⟩ direction. At 0.4 MeV and for the (110) and (111) orientations, the calculated fraction of interstitials which are created in the ⟨100⟩ direction with an energy sufficient to undergo more than the minimum number of lens passages is very small (6.5% if $T_d^{\langle 100\rangle} = 16.5$ eV, 2.5% if it is 17 eV). Thus, the observed recovery between 90 and 100 K (first part of I_D), which amounts to

TABLE II. The contributions of the ⟨111⟩ displacements to the total cross section computed with various $T_d^{\langle 100\rangle}$ and $T_d^{\langle 111\rangle}$ compared with the (to 125 K normalized) recovery during the second part of I_{D+E}— case (a), and with the recovery during the substage I_C *plus* the second part of I_{D+E}— case (b), for three iron crystals at various electron energies.

		(a)		(b)	
E(MeV)	(hkl)	σ(111) in % with $T_d\langle 100\rangle = 17$ eV and $T_d\langle 111\rangle = 20$ eV	% $\Delta\rho/\Delta\rho_{125\ K}$ at 100–125 K	σ(111) in% with $T_d\langle 100\rangle = 16.5$ eV and $T_d\langle 111\rangle = 19$ eV	% $\Delta\rho/\Delta\rho_{125\ K}$ at 75–90 K plus 100–125 K
0.4	(100)	9	8	18.5	26
	(110)	19.5	19	33.5	37
	(111)	32	25	47	43
0.45	(100)	30	17	36.5	33
	(110)	41.5	27	45.5	45
	(111)	49.5	30	50.5	49
0.65	(100)	69	35	71.5	59
	(110)	46.5	33	47.5	52
	(111)	35	25	36	44

more than half of state I_B—cf. Fig. 6(c)—cannot, in this case, be attributed to distant ⟨100⟩ pairs. This recovery could be related to a different configuration of the ⟨100⟩ pairs, as in the case of molybdenum.[7] However, a more detailed study of the recovery after a very low-energy irradiation is needed before drawing any definite conclusion. Moreover, one must not forget that the various substages between 75 and 125 K are not entirely separated and that, in the regions of overlap, processes of different origins may take place at the same time.

5. *Comparison with molybdenum*

Although the stage-I recovery for iron is taking place in a temperature range which is much higher than for molybdenum[6]—or other bcc metals like chromium[28] for example—some common features can be noted: the first important substage can be attributed to close Frenkel pairs produced in the ⟨100⟩ direction; the following substage is likely to be due to ⟨111⟩ close pairs; substage I_D is the most important one. However, in the case of iron, it cannot be attributed to ⟨100⟩ pairs only, as it was done for molybdenum. The recovery of ⟨100⟩ pairs and that of the ⟨111⟩ pairs in this range are superposed, although, on the average, the ⟨100⟩ pairs anneal at a slightly lower temperature than the ⟨111⟩ pairs.

Thus, there do not exist, in the case of iron, two "brother peaks" like the two peaks at 15 K and 40 K observed in molybdenum. These two peaks had been interpreted[29] as related to two different configurations of the ⟨100⟩ Frenkel pairs. The difference between these two configurations stems from the anisotropy of the relaxation field around the vacancy. Besides, Kenny *et al.*,[30] who had calculated the relaxation field around a vacancy in Fe, Mo, and V, have found that the distortion is much smaller in the case of iron. This effect which originates in the interatomic potential gives rise to a much less anisotropic strain field, due to the vacancy, around an interstitial created in a ⟨100⟩ direction and could explain the difference between the two recovery spectra. This has to be checked by similar calculations as those worked out for molybdenum.

CONCLUSIONS

We have irradiated single crystals of iron and measured the defect production rate as a function of the incident electron energy for three crystallographic orientations of the samples. A geometrical model for the threshold-energy surface allows us to fit the experimental data reasonably well and leads to the following values for the threshold energies in the main crystallographic directions:

$$T_d^{\langle 100\rangle} = 17 \pm 1 \text{ eV}, \quad T_d^{\langle 111\rangle} = 20 \pm 1.5 \text{ eV},$$

$$T_d^{\langle 110\rangle} \gtrsim 30 \text{ eV}.$$

The Frenkel-pair resistivity is deduced to be $\rho_F^{Fe} = 30 \pm 5\ \mu\Omega\text{cm/at.\%}\ F.P.$

From the obtained threshold energies, we derived an interatomic potential of the Born-Mayer type, valid in the range $1.2 < r < 2.5$ Å. Our best choice is

$$V(r) = 8900\ e^{-4.5r} \text{ eV}.$$

We have also measured the isochronal recovery of the defects after irradiations at different en-

ergies. The first important substage, which is centered at 66 K (I_B), is shown to be clearly related with close Frenkel pairs created in the ⟨100⟩ direction (which is also the direction of minimum threshold energy for displacement). The interpretation of substate I_C, centered at ~87 K, is not straightforward, since it appears not to depend much on the energy or on the sample orientation. The comparison with the calculated cross sections suggests that it could be due to ⟨111⟩ close pairs. Substage I_D, from 90 to 110 K, is complex. Its first part (below 100 K) stems mostly from ⟨100⟩ pairs whilst the second part (above 100 K), together with substage I_E, stems from ⟨111⟩ pairs, principally. The whole substage I_D is not incompatible with the correlated recombination of the free interstitial.

ACKNOWLEDGMENTS

We wish to thank Professor Y. Cauchois, head of the Laboratory, who made this work possible. We are grateful to Dr. B. Thomas of the IRSID (St. Germain en Laye) who kindly offered his iron crystals, and to D. L. Thomé (Institut de Physique Nucléiare, Orsay) for his aid in their preparation. The technical assistance of the accelerator team was appreciated.

* Laboratoire de Physique de l'Ecole Normale Supérieure de Jeunes Filles, F-92120 Montrouge, France.

[1] J. B. Gibson, A. N. Goland, M. Milgram, and G. H. Vineyard, Phys. Rev. 120, 1229 (1960).
[2] C. Erginsoy, G. H. Vineyard, and A. Englert, Phys. Rev. 133, A595 (1964).
[3] P. Vajda (unpublished).
[4] J. N. Lomer and M. Pepper, Philos. Mag. 16, 1119 (1967).
[5] P. Jung and W. Schilling, Phys. Rev. B 5, 2046 (1972).
[6] M. Biget, P. Vajda, A. Lucasson, and P. Lucasson, Radiat. Eff. 21, 229 (1974).
[7] F. Maury, P. Vajda, M. Biget, A. Lucasson, and P. Lucasson, Radiat. Eff. 25, 175 (1975).
[8] Y. Cusson, P. Lucasson, and R. M. Walker, *Proceedings of the International Conference on the Properties of Reactor Material, Berkeley*, 1961 (Butterworths, London, 1961).
[9] F. Dausinger, H. Schultz, Proceedings of the International Conference on the Fundamental Aspects of Radiation Damage in Metals, Gatlinburg, 1975, Vol. I, p. 438 (Conf.-751006-P1) (unpublished).
[10] P. Lucasson, A. Lucasson, and G. Lelogeais, Cryogenics 6, 169 (1966).
[11] A. Sato and M. Meshii, Phys. Status Solidi A 22, 253 (1974).
[12] N. F. Mott and H. S. W. Massey, *The Theory of Atomic Collisions* (Clarendon, Oxford, 1949), p. 195.
[13] P. Lucasson and R. M. Walker, Phys. Rev. 127, 485 (1962).
[14] F. Maury, Thesis, Univ. of Paris at Orsay, No. 1076 (1973) (unpublished).
[15] W. Dönitz, W. Hertz, W. Waidelich, H. Peisl, and K. Böning, Phys. Status Solidi A 22, 501 (1974).
[16] J. A. Horak and T. H. Blewitt, Phys. Status Solidi A 9, 721 (1972).
[17] G. Lück and R. Sizmann, Phys. Status Solidi 5, 683 (1964).
[18] H. H. Andersen and P. Sigmund, DAEC Risö Rep. No. 103 (1965) (unpublished).
[19] A. A. Abrahamson, Phys. Rev. 178, 76 (1969).
[20] R. A. Johnson, Phys. Rev. 134, A1329 (1964).
[21] R. Bullough and R. C. Perrin, *Radiation Damage in Reactor Materials*, Vol. II, (IAEA, Vienna, 1969).
[22] L. A. Girifalco and V. G. Weizer, Phys. Rev. 114, 687 (1959).
[23] C. Minier-Cassayre, Thesis (University of Grenoble, CEA-R-2905, 1966) (unpublished).
[24] H. H. Neely and D. W. Keeffer, Phys. Status Solidi 24, 217 (1967).
[25] J. L. Leveque, T. Anagnastopoulos, H. Bilger, and P. Moser, Phys. Status Solidi 31, K47 (1969).
[26] J. M. Wells, K. C. Russel, Radiat. Eff. 28, 157 (1976).
[27] J. Verdone, W. Chambron, and P. Moser, Phys. Status Solidi B 61, K41 (1974).
[28] M. Biget, P. Vajda, F. Maury, A. Lucasson, and P. Lucasson, Proceedings of the International Conference on the Fundamental Aspects of Radiation Damage in Metals, Gatlinburg, 1975, Vol. I, p. 66 (Conf.-751006-P1) (unpublished).
[29] F. Maury and P. Lucasson, Phys. Status Solidi A 34, 513 (1976).
[30] P. N. Kenny, A. J. Trott, and P. T. Heald, J. Phys. F 3, 513 (1973).